Cerebral Cortex September 2010;20:2043–2054
doi:10.1093/cercor/bhp267
Advance Access publication January 6, 2010

Proper Layering Is Important for Precisely Timed Activation of Hippocampal Mossy Cells

Janina Kowalski[1–4], Markus Geuting[1], Sebastian Paul[1], Sandra Dieni[1], Jean Laurens[5], Shanting Zhao[1], Alexander Drakew[1], Carola A. Haas[2,6], Michael Frotscher[1–3] and Imre Vida[2,7]

[1]Institute of Anatomy and Cell Biology, Department of Neuroanatomy, [2]Bernstein Center for Computational Neuroscience, [3]Spemann Graduate School of Biology and Medicine, [4]Faculty of Biology, University of Freiburg, D-79104 Freiburg, Germany, [5]Department of Neurology, Zürich University Hospital, CH-8091 Zürich, Switzerland, [6]Experimental Epilepsy Research, Neurocenter, University of Freiburg, D-79106 Freiburg, Germany and [7]Neuroscience and Molecular Pharmacology, Faculty of Biological and Life Sciences, University of Glasgow, Glasgow G12 8QQ, UK

Address correspondence to Imre Vida, Neuroscience and Molecular Pharmacology, Faculty of Biological and Life Sciences, University of Glasgow, West Medical Building, Glasgow G12 8QQ, UK. Email: i.vida@bio.gla.ac.uk.

The mammalian cortex exhibits a laminated structure that may underlie optimal synaptic connectivity and support temporally precise activation of neurons. In *'reeler'* mice, the lack of the extracellular matrix protein Reelin leads to abnormal positioning of cortical neurons and disrupted layering. To address how these structural changes impact neuronal function, we combined electrophysiological and neuroanatomical techniques to investigate the synaptic activation of hippocampal mossy cells (MCs), the cell type that integrates the output of dentate gyrus granule cells (GCs). While somatodendritic domains of wild-type (WT) MCs were confined to the hilus, the somata and dendrites of reeler MCs were often found in the molecular layer, where the perforant path (PP) terminates. Most reeler MCs received aberrant monosynaptic excitatory input from the PP, whereas the disynaptic input to MCs via GCs was decreased and inhibition was increased. In contrast to the uniform disynaptic discharge of WT MCs, many reeler cells discharged with short, monosynaptic latencies, while others fired with long latencies over a broad temporal window in response to PP activation. Thus, disturbed lamination results in aberrant synaptic connectivity and altered timing of action potential generation. These results highlight the importance of a layered cortical structure for information processing.

Keywords: action potential timing, cortical lamination, dentate gyrus, reeler mutant, synaptic transmission

Introduction

The dentate gyrus (DG) serves as the gateway to the hippocampus and plays an essential role in spatial navigation and the acquisition of new memories (Burgess et al. 2002). It is also thought to act as a filter that prevents the propagation of overt excitation to the sensitive CA3 area (Heinemann et al. 1992). Proper DG function is critically dependent on hilar mossy cells (MCs), which integrate DG output and provide feedback to set the balance of excitation and inhibition in this region (Buckmaster and Schwartzkroin 1994; Ratzliff et al. 2002; Sloviter et al. 2003).

Similar to other cortical areas, the DG has a distinct laminated structure (Förster et al. 2006; Frotscher et al. 2007). The main afferent system from the entorhinal cortex, the perforant path (PP), forms a bundle and innervates the distal dendrites of granule cells (GCs) in the outer molecular layer. In contrast, the MC axons that form the commissural/associational pathway terminate on proximal GC dendrites in the inner molecular layer (Deller et al. 1999). Different cell populations also show segregated distribution: GC bodies form a densely packed somatic layer, whereas MCs are confined to the hilus. Although the functional relevance of this laminar organization remains unknown, a plausible explanation is that lamination minimizes the length of axons and dendrites while maximizing the number of synaptic connections (Chklovskii 2004). Such "optimal wiring" of the network is likely to be crucial for the efficient, temporally precise activation of neurons (Schmidt-Hieber et al. 2007).

Cortical lamination is disrupted in Reelin deficiency, for example, in *'reeler'* mutant mice (Falconer 1951; D'Arcangelo et al. 1995) and human patients with a form of lissencephaly (Hong et al. 2000). The lack of Reelin results in migration defects leading to abnormal positioning and morphology of neurons. In the reeler DG, GCs lose their alignment and become scattered throughout the hilus (Drakew et al. 2002). Afferent pathways are differentially affected; the PP remains bundled in the outer molecular layer (Borrell, Del Rio, et al. 1999), but commissural/associational fibers terminate diffusely in the hilus and inner molecular layer (Zhao et al. 2003). Despite the altered layering, it was previously reported that specificity of synaptic connections is maintained (Stirling and Bliss 1978; Deller et al. 1999; Drakew et al. 2002). Electrophysiological recordings further showed that synaptic responses are largely unchanged in the hippocampus (Bliss and Chung 1974; Ishida et al. 1994). However, more recently, it was proposed that the reeler dentate-hilar network displays an abnormal excitatory connectivity and a propensity for seizures (Patrylo et al. 2006). Thus, the functional impact of disrupted layering remains unknown.

In a previous immunocytochemical work, we noted potential changes in MC morphology in reeler mice (Drakew et al. 2002). In the present study, we therefore investigated how anatomical and physiological properties of MCs are affected. Our results reveal that not only are the localization and morphology of these cells dramatically changed, but they also receive an aberrant excitatory input. However, while reeler MCs do not show enhanced excitability, they do exhibit altered temporal activation with a high degree of heterogeneity.

Materials and Methods

Immunofluorescent Labeling

For immunocytochemical investigations, 2 reeler (The Jackson Laboratory, Bar Harbor, ME, B6C3Fe background) and 2 wild-type (WT) littermate mice (3 months old) were deeply anesthetized with Narkodorm-n (180 mg/kg, intraperitoneal; Alvetra, Neumünster, Germany). The vascular system was flushed with 0.9% saline for 1 min, followed by transcardial perfusion with a fixative solution

containing 4% paraformaldehyde (PFA) in 0.1 M PB (80 mL for 13 min). After perfusion, brains were removed and tissue blocks containing the hippocampus were sectioned at 50 μm on a vibratome. Sections were rinsed several times in phosphate-buffered saline (PBS, 0.025 M, pH 7.3) before incubation in the primary antibody against calretinin (CR, mouse monoclonal, Swant, Bellinzona, Switzerland; 1:5000 dilution in PBS containing 5% goat serum and 0.3% triton X-100) for 48 h at 4 °C. The sections were rinsed in PBS, then incubated in the secondary antibody solution (goat anti-mouse, conjugated with Alexa 488, Invitrogen Corporation, Carlsbad, CA; 1:500 dilution in PBS and 0.3% triton X-100) for 4–6 h at 22 °C. Sections were counterstained with the nuclear dye 4′,6-diamidino-2-phenylindole (dilution 1:500) included in the secondary antibody solution. Finally, sections were mounted on glass slides in a fluorescent mounting medium (Prolong Antifade, Molecular Probes Eugene, OR) under coverslips and examined with an Olympus BX61 microscope equipped with epifluorescent illumination and a digital camera system (Cell F Software package, Olympus Soft Imaging Solutions, Münster, Germany). Low-power images of the DG were created using the extended focal image function of the software. Additionally, the immunoreactivity was analyzed using a ×40 oil immersion objective (numerical aperture 1.3) on a confocal microscope system (LSM 510, Carl Zeiss GmbH, Oberkochen, Germany).

Animals and Tissue Preparation for Electrophysiology

For the intracellular labeling and electrophysiological characterization, 18- to 49-day-old reeler (42 animals) and WT mice (13 B6C3Fe reln +/+ littermates and 30 C57Bl/6 mice) were used. After deep anesthetization with isoflurane, the animals were killed by decapitation in accordance with international and institutional guidelines. The brains were instantly removed and immersed in ice-cold artificial cerebrospinal fluid (ACSF). Horizontal 300-μm slices were cut using a DSK 1000 vibratome (Dosaka Co. Ltd., Kyoto, Japan) and subsequently incubated at 37 °C for at least 40 min in low-calcium ACSF solution. For electrophysiological recording, slices were transferred to a recording chamber and superfused with standard ACSF solution at a rate of 2–3 mL/min. The standard ACSF was composed of (in mM): 125 NaCl, 25 $NaHCO_3$, 25 glucose, 2.5 KCl, 1.25 NaH_2PO_4, 2 $CaCl_2$, and 1 $MgCl_2$ and equilibrated with 95% O_2 and 5% CO_2; composition of the low-calcium ACSF was identical except for $CaCl_2$ which was reduced to 0.5 mM and $MgCl_2$ which was increased to 4 mM. All experiments were performed at near physiological temperatures of 31–34 °C. The experiments were performed with knowledge of the genotype of the mice due to the obvious differences in the phenotype and cytoarchitecture between reeler and WT.

Whole-Cell Patch-Clamp and Extracellular Recordings

Somatic whole-cell patch-clamp recordings were made from visually identified cells using infrared differential interference contrast video microscopy on an upright microscope equipped with a ×40 water immersion objective (Zeiss, Oberkochen, Germany) and video camera (C2400-07, Hamamatsu, Hamamatsu City, Japan).

Patch pipettes were pulled from borosilicate glass tubing (2-mm outer diameter, 1-mm inner diameter) on a Sutter P-87 puller (Sutter Instrument Company, Novato, CA). The intracellular pipette solution contained (in mMol): 120 K-gluconate, 20 KCl, 2 $MgCl_2$, 10 ethyleneglycol-bis(2-aminoethylether)-N,N,N',N'-tetra acetic acid, 10 4-(2-hydroxyethyl)-1-piperazineethanesulfonic acid (HEPES), 2 Na_2ATP, as well as 0.2–0.3% biocytin. For the characterization of synaptic responses, 18 mMol of KCl were substituted with K-gluconate in the pipette solution. The resistance of the filled electrodes was between 2 and 5 MΩ. During voltage-clamp (VC) recordings of synaptic responses, the cells were held at −50 mV, and the mean series resistance (R_s, range: 5–26 MΩ) was compensated by 75–80%. Nevertheless, VC errors and space-clamp errors (Spruston et al. 1993; Williams and Mitchell 2008) in the extensive dendritic structure of MCs may be substantial and could compromise kinetic and amplitude estimates of distal synaptic events such as PP excitatory postsynaptic currents (EPSCs). Cells with a change in R_s of 20% or more during the recording were excluded from the analysis. Current-clamp (CC) recordings were made at resting membrane potential, and R_s was fully compensated. Only neurons with a stable resting membrane potential of at least −50 mV and an overshooting action potential (AP) were included in the evaluation. No junction potential compensation was applied to the data.

For extracellular (EC) field potential recordings, electrodes were filled with HEPES-buffered physiological NaCl solution and had resistances between 0.2 and 5 MΩ. The electrodes were placed in the GC layer at the DG crest in WT and at a corresponding location in the GC-rich border region of the hilus in reeler slices.

Synaptic responses were elicited by EC stimulation by a monopolar electrode (glass pipettes filled with HEPES-buffered physiological NaCl solution, resistance: 0.1–1.8 MΩ) placed in the outer molecular layer (close to the fissure) at the DG crest where the PP fibers enter the area. Stimuli were generated using a DS3 constant current isolated stimulator (Digitimer Ltd, Hertfordshire, UK). Paired stimuli with 50-ms intervals were applied, and traces were collected at 0.1 Hz. During VC recordings, the stimulus intensity was set to a value below the threshold for generating an EC population spike (PS) at the first stimulus, but at a sufficient threshold to generate a PS at the second stimulus (nominal 25–150 μA, 0.1 ms). To maximize activation during CC recordings, stimulus intensities were increased to elicit a PS already at the first stimulus (80 μA –3.2 mA, 0.1 ms). Cells activated antidromically by the stimulus were excluded from the analysis. Excitatory amino acid blockers 6-Cyano-7-nitroquinoxaline-2,3-dione disodium (CNQX, 10 μM) and D-(-)-2-Amino-5-phosphonopentanoic acid (D-AP5, 50 μM, Biotrend, Zurich, Switzerland) were bath applied to pharmacologically isolate monosynaptic inhibitory postsynaptic currents (IPSCs), while the γ-aminobutyric acid $(GABA)_A$ receptor blocker 1(S),9(R)-(-)-Bicuculline methiodide (10 μM, Sigma-Aldrich, St Louis, MO) was used to isolate EPSCs.

Recordings were performed using Axopatch 200B amplifiers (Axon Instruments, Union City, CA) in VC or fast CC mode. Signals were filtered at 5–10 kHz using the integrated 4-pole low-pass Bessel filter of the amplifier and digitized at 10–20 kHz. Data were collected using the EPC software (CED, Cambridge, UK) and pClamp 9.2 (Axon Instruments) software packages running on Pentium PCs.

Electrophysiological Data Analysis

The resting membrane potential of the recorded neurons was determined shortly after breaking in. Input resistance was calculated by plotting the steady state of the 200-ms voltage responses against the amplitude of the current pulses within a range of ±40 pA. To determine membrane time constants, the decay of the averaged voltage response (360 traces) to a brief current pulse (1 ms, –0.5 nA) was fitted by a monoexponential function using the Levenberg-Marquardt/sum of squared errors method. Membrane capacitance was taken as the nominal value of the cell capacitance compensation applied to the amplifier during VC recording. AP parameters were always determined from the first APs in response to small suprathreshold current pulses (≤120 pA, 200–400 ms). AP threshold was defined as the membrane potential at which the first derivative of the rising phase first exceeded 20 mV/ms. The peak amplitude of APs and fast after-hyperpolarisation (AHP) were measured from threshold. In a few cells, the fast and medium AHPs merged, and no negative peak could be detected immediately after the AP. In these cells, the amplitude of the fast AHP was taken at the time point where the first derivative of the repolarizing phase dropped below 1 mV/ms. Half-height duration represents the duration of the AP at half-maximal amplitude. The maximal rates of rise and decay were determined from the first derivative (dV_m) of the AP waveform. Firing frequency was determined in responses to 200 pA, 200 ms depolarizing current pulses.

EPSC amplitudes were measured from the level directly preceding the onset of the EPSC in averages of at least 6 evoked responses. Absolute latencies of EPSCs and IPSCs were measured from the time of the stimulus to the onset of the event in averaged responses. The relative latency of the events from the EC PS was measured from the PS onset to the event onset in the averages. Negative values indicate that the event precedes the PS. Stimulus-dependent firing was determined in a 30-ms time interval after each stimulus. Latencies of APs were measured from the time of the stimulus to the time of threshold crossing in individual traces. Decay time constants of EPSCs and

IPSCs were determined by fitting a monoexponential function using the Levenberg-Marquardt/sum of squared errors method. Firing probabilities were calculated from 15 or more consecutive evoked responses. Data analysis and evaluation were performed using the pClamp software package, the open source analysis program Stimfit (http://www.stimfit.org; courtesy of Dr C. Schmidt-Hieber) and custom-made routines in Matlab 7.1 (The MathWorks Inc., Natick, MA).

Visualization and Morphological Analysis

Morphological analysis of MCs was performed as previously reported (Vida and Frotscher 2000). In brief, neurons were filled with biocytin (0.1–0.3%) during electrophysiological recording. Slices were immersion-fixed overnight in a phosphate-buffered solution (100 mM PB, pH 7.4) containing 2.5% PFA and 1.25% glutaraldehyde. Filled cells were visualized using avidin–biotin–peroxidase complex and 3,3′-diaminobenzidine tetrahydrochloride as the chromogen. After visualization, the slices were either directly embedded in an aqueous mounting medium (Mowiol, Sigma-Aldrich, Taufkirchen, Germany) or processed further for electron microscopic analysis. For this purpose, slices were resectioned on a vibratome at 50–70 μm thickness. The sections were postfixed in 1% osmium tetroxide in PB (30 min), dehydrated between coverslips in an ascending series of ethanol and transferred to propylene oxide (2 × 10 min). Sections were embedded in Durcopan (Fluka, Buchs, Switzerland) overnight, mounted under coverslips and left to polymerize at 56 °C for 48 h. Filled neurons were examined on a light microscope (Zeiss Axophot) using ×40 and ×63 oil immersion objectives (numerical aperture 1.3–1.4) and reconstructed and analyzed using the Neurolucida software package (MicroBrightField, Williston).

For electron microscopy, areas of the molecular layer including biocytin-labeled ectopic dendrites of reeler MCs were reembedded. Serial ultrathin sections were cut and mounted on single-slot Formvar-coated copper grids and contrasted with lead citrate. Sections were examined in the electron microscope (LEO 906 E, Zeiss). Synaptic junctions were identified on the basis of characteristic widening of the EC space between 2 opposing, parallel membrane specializations (synaptic clefts) of a biocytin-labeled dendrite or spine and a presynaptic bouton. Additional criteria were: the accumulation of vesicles in the presynaptic element at putative release sites and electron-opaque material in the synaptic cleft.

Statistics

Values are given as mean ± standard error of the mean. Statistical evaluation was performed using either Matlab 7.1 or the R software package (GNU R Project, http://www.r-project.org). Differences were assessed by the Wilcoxon signed-rank or the Wilcoxon rank-sum (Mann–Whitney–Wilcoxon) tests for paired and unpaired samples, respectively. Familywise error rate was corrected for by the Holm–Bonferroni method. No differences were observed in morphological properties, spontaneous and evoked synaptic responses, and passive electrophysiological parameters of the 2 WT groups; these data were pooled. Differences were noted in the AP waveform between the 2 groups; therefore, active physiological properties are reported from WT littermate cells only (Table 1).

Table 1
Intrinsic physiological properties of WT and reeler MCs

	WT	Reeler	*P* value
Resting membrane potential (Vm)	−62.9 ± 0.8 (66)[a]	−61.7 ± 0.5 (81)	0.535
Input resistance (MΩ)	270 ± 19 (22)[a]	247 ± 11 (49)	0.250
Membrane time constant (ms)	48 ± 3 (24)[a]	49 ± 2 (48)	0.582
Membrane capacitance (pF)	47 ± 2 (46)[a]	49 ± 1 (80)	0.445
AP			
Threshold (ms)	−41.8 ± 0.7 (18)[b]	−41.3 ± 0.3 (81)	0.680
Amplitude (mV)	90.2 ± 1.0 (18)[b]	91.8 ± 0.5 (81)	0.078
Half-height duration (ms)	0.70 ± 0.02 (18)[b]	0.64 ± 0.01 (81)	0.039
Maximum rate of rise (mV/ms)	401 ± 16 (18)[b]	452 ± 8 (81)	0.001*
Maximum rate of repolarization (mV/ms)	118 ± 4 (18)[b]	130 ± 2 (81)	0.017
Afterhyperpolarization (mV)	7.1 ± 0.4 (18)[b]	9.4 ± 0.3 (81)	<0.001*
Discharge frequency	38 ± 5 (11)[b]	31 ± 2 (54)	0.270

Note: Values are expressed as mean ± standard error of the mean; number of cells is indicated in parenthesis. Asterisks indicate significant differences between the WT and reeler groups assessed using the Holm–Bonferroni correction.
[a]Pooled WT data set.
[b]WT littermate data only. For further details, see Materials and Methods.

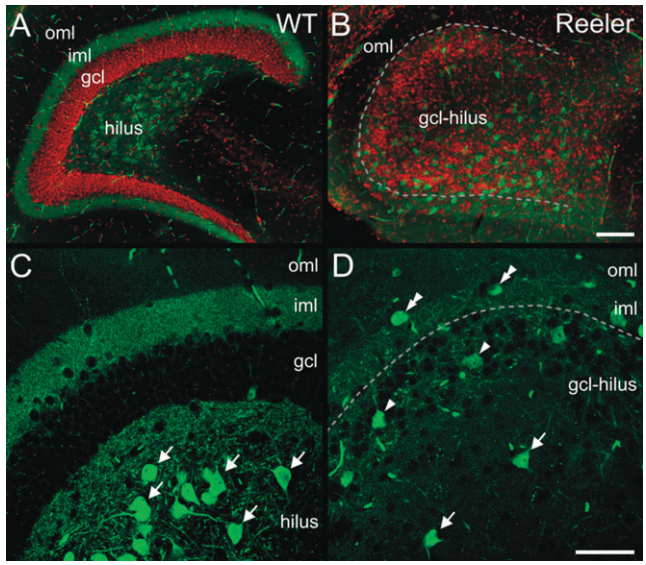

Figure 1. Immunofluorescent staining for CR reflects the disrupted layering of the reeler DG. (*A*) Low-power photomicrograph of a horizontal section from the ventral hippocampus shows the laminar distribution of CR immunoreactivity (green) in WT mice. The immunostaining highlights the MC somata in the hilus, while the labeled MC axons of the associational/commissural pathway are observed as a homogenous band in the inner molecular layer (iml), forming sharp borders at the GC layer (gcl) and the outer molecular layer (oml). The section is counterstained with the nuclear dye 4′,6-diamidino-2-phenylindole to visualize the distribution of cellular nuclei (red pseudocolor), thus revealing the densely packed GC somata in the gcl. (*B*) In a section of reeler ventral hippocampus, the laminar arrangement of CR immunoreactivity is disrupted, whereby a well-defined border between the gcl and the hilus (gcl–hilus) is lacking. (*C*, *D*) High-power confocal images of CR-immunolabeled sections. Immunopositive cell bodies of putative MCs are confined to the central hilus in the WT (*C*, arrows), whereas in the reeler, cell bodies are scattered in the center and the cell-rich periphery of the hilus (*D*, arrows and arrowheads), as well as in the iml (double arrowheads). Scale bars: *A*, *B*—100 μm; *C*, *D*—50 μm.

Results

Layered Distribution of CR Immunoreactivity Is Disrupted in Reeler Mice

Majority of MCs in the murine ventral hippocampus express the calcium-binding protein CR (Liu et al. 1996). Therefore, to compare the distribution of MCs in WT and reeler mice, we first performed immunofluorescent labeling against this protein (Fig. 1). In horizontal sections from the ventral hippocampus of WT mice, CR immunoreactivity showed a laminar distribution pattern, with clear demarcation of both the hilus and the inner molecular layer (Fig. 1*A*). In the hilus, a central cluster of large, immunopositive cell bodies was visible, while at higher magnification, numerous large-caliber, immunopositive processes resembling dendrites were observed (Fig. 1*C*, arrows). In the inner molecular layer, a dense meshwork of CR-positive axon collaterals manifested as a homogeneous band of immunoreactivity (Fig. 1*A*,*C*). Additionally, a low number of CR-immunopositive interneurons were found scattered in the DG; these cells could be distinguished from MCs on the basis of their morphological

features (e.g. small round somata, smooth dendrites, and the lack of complex spines). The overall staining pattern for CR was dominated by the immunoreactivity corresponding to cell bodies, dendrites, and axons of MCs, as described previously (Liu et al. 1996; Blasco-Ibanez and Freund 1997).

In reeler mice, the characteristic laminar pattern of CR immunostaining was severely disrupted (Fig. 1*B,D*). Large immunopositive cell bodies were found not only scattered throughout the central hilus, but also among the dispersed GCs and in the inner molecular layer (Fig. 1*D*, arrowheads). In addition, immunolabeling of axons in the molecular layer was found to be reduced and dispersed compared with the WT hippocampus (Fig. 1*D*). Although some CR-positive elements are not MCs, these results clearly indicate that the localization and morphology of MCs are markedly altered in reeler mice (Borrell, Ruiz, et al. 1999; Coulin et al. 2001; Drakew et al. 2002).

Reeler MCs Show Altered Somal Localization and Aberrant Dendritic Distribution

To investigate the morphological changes in MCs at the single-cell level, we next performed whole-cell patch-clamp recordings in combination with intracellular labeling in acute slices from WT and reeler mice. The recorded neurons were subsequently visualized and analyzed under the light microscope (Fig. 2). In WT slices, the somata and dendrites of MCs were observed in the hilus (Fig. 2*A*). A characteristic feature of these cells is the presence of large complex spines, the so-called "thorny excrescences," on the proximal dendrites (Fig. 2*D*, arrows). By performing 3-dimensional reconstructions of WT MCs, we confirmed that essentially all WT MC dendrites were confined to the hilus (Fig. 2*G*).

In reeler mice, both the localization and morphology of MCs was different to that observed in the WT and showed strong heterogeneity (Fig. 2*B,C*). Reeler MCs were found not only in the hilus (Fig. 2*B,H*), but also in the GC-rich zone and inner molecular layer (Fig. 2*C,I*), thus corroborating our immunocytochemical findings. Additionally, the dendritic tree of these cells consistently extended into the molecular layer, independent of the somal position (Fig. 2*B,C,H,I*). Despite the observed changes in localization and morphology, MCs could still be unequivocally identified on the basis of their complex spines (Fig. 2*E,F*, arrows).

In both WT and reeler slices, only very little axon of the labeled MCs was found in the hilus and molecular layer, as major axon collaterals were mostly cut on the surface of the slices. This is consistent with the fact that MCs preferentially project to distal septotemporal levels of the ipsilateral and to the contralateral hippocampus (Amaral and Witter 1989; Buckmaster et al. 1996). In view of the limited extent of the axon preserved in the slices, we have not analyzed it in further detail.

To further characterize the morphological differences between WT and reeler MCs, we next analyzed the dendritic tree of the reconstructed neurons quantitatively. Surprisingly, despite the clear morphological differences, the mean values for total dendritic length were very similar between the 2 groups (5392 ± 313 μm, 13 WT vs. 5054 ± 517 μm, 9 reeler neurons; Fig. 2*J*). Similarly, the size of the soma was comparable in WT and reeler MCs (the largest diameter was 25.5 ± 1.0 μm and 23.3 ± 1.2 μm, respectively). In contrast, the laminar distribution of the dendrites differed between WT and reeler MCs. From WT MCs, only 2 cells had 2 short dendrites each extending into the molecular layer. Conversely, all reeler MCs had several dendritic segments (mean 27 ± 6) in this layer. Accordingly, the proportion of the total dendritic length in the molecular layer was much higher for reeler MCs (44 ± 11%) than for WT cells (0.4 ± 0.01%, $P < 0.001$, Fig. 2*K*). However, reeler MCs also showed a high degree of cell-to-cell variability, and MCs located in the inner molecular layer had more dendrites in the molecular layer (36–88% of total length), whereas MCs positioned in the hilus typically had less dendrites (8–30%) in this layer.

Further differences between WT and reeler groups were revealed by analysis of the dendritic branching pattern. The total number of dendritic segments was lower in reeler (66 ± 7) than in WT (80 ± 5, $P = 0.03$). In WT MCs, low-order dendrites were short and showed regular branching. The number of dendritic segments peaked in the third and fourth orders (total of 38 ± 2, Fig. 2*L*), and these branch orders accounted for 51% of the total dendritic length (Fig. 2*M*). In contrast, the first- and second-order dendritic segments in reeler MCs were significantly longer (mean segment length was 88 ± 12 μm vs. 48 ± 7 μm in WT, $P = 0.002$), and many low-order dendrites terminated without further branching. Consequently, the number of third- and fourth-order dendritic segments (total: 24 ± 2, $P = 0.001$; Fig. 2*L*) was lower, and the corresponding cumulative dendritic length accounted for an average of only 37% of the total (Fig. 2*M*, $P = 0.001$), indicating a redistribution of the dendritic surface in reeler MCs. In conclusion, while the reeler MC dendrites do not show a change in total length, their laminar distribution is altered and the complexity of branching reduced compared with WT MCs.

To see if the ectopic dendrites receive synaptic inputs, we performed electron microscopic analysis of 2 biocytin-filled reeler MCs. Soma and proximal dendrites of one of these cells were located in the inner molecular layer. Electron microscopic examination showed that the complex spines emerging from these dendrites were engulfed by large presynaptic terminals characteristic of mossy fiber boutons (5 boutons examined; Fig. 3*A*). In contrast, in the outer molecular layer, where the majority of axons belong to the PP (Borrell, Del Rio, et al. 1999), simple spines emerged from the distal dendrites and formed contacts with small presynaptic boutons (15 synaptic contacts; Fig. 3*B,C*). Similarly, in the case of a MC with its soma in the hilus, synaptic contacts were found between distal dendritic spines and putative PP axons in the outer molecular layer (14 synaptic contacts; Fig. 3*D,E*). Additionally, synaptic contacts were found on distal dendritic shafts of both MCs analyzed (15 synaptic contacts examined from the 2 MCs; Fig. 3*F*). Many of these shaft synapses may represent the inhibitory input; however, a putative identification was not possible due to the opaque peroxidase reaction end product masking the postsynaptic membrane. These results indicate that ectopic dendrites of reeler MCs receive synaptic input. Similar to WT MCs (Amaral 1978; Ribak et al. 1985), mossy fibers form synapses with complex spines on the proximal dendrites of reeler MCs even in the inner molecular layer. However, the presence of synaptic contacts onto the ectopic distal dendrites in the PP termination zone suggests that they also receive aberrant excitatory input from this afferent system.

Intrinsic Properties of Reeler MCs

To identify possible changes in the physiological properties of MCs, we next determined the intrinsic properties of the cells

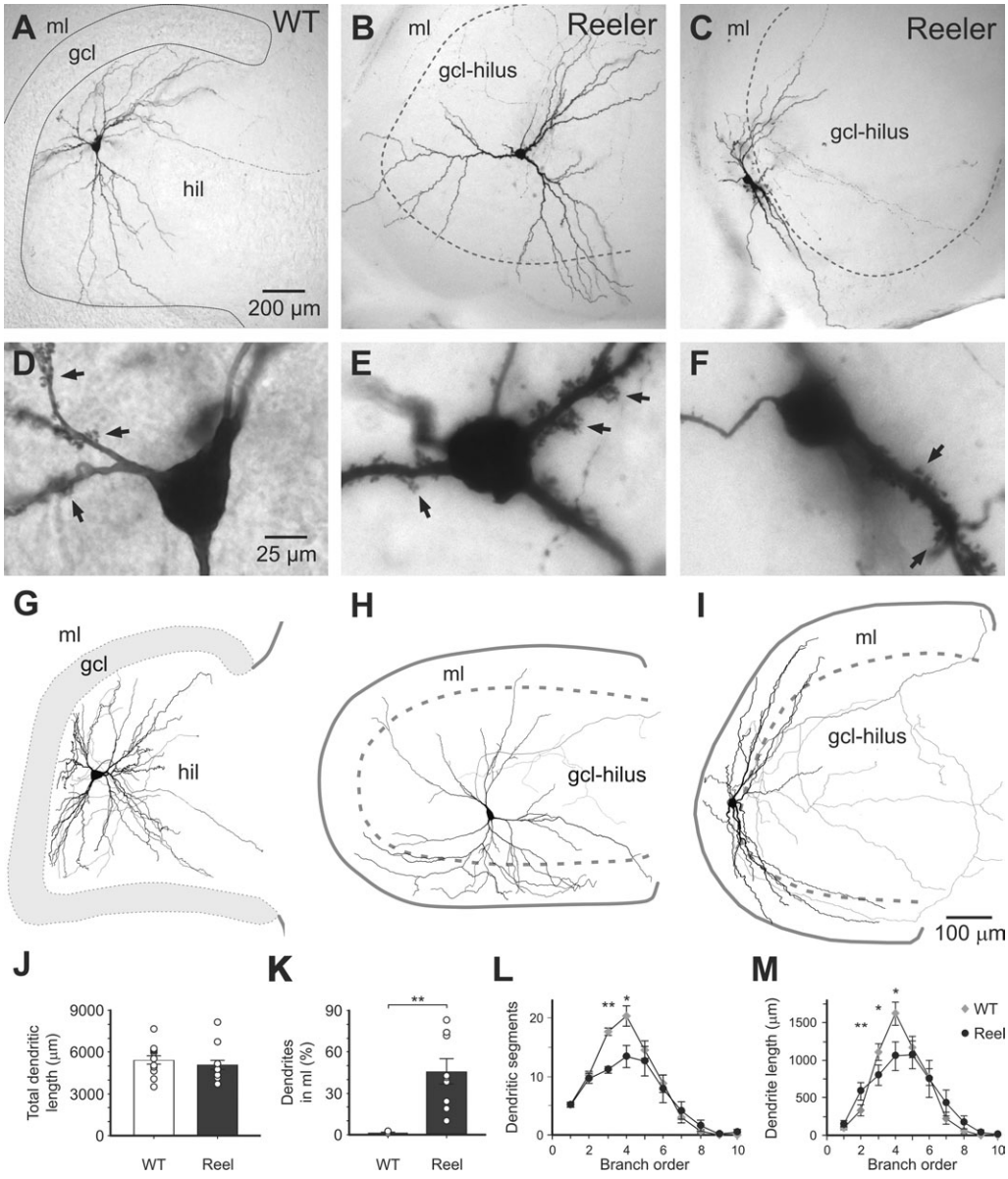

Figure 2. Altered position and somatodendritic morphology of MCs in reeler mice. (*A–C*) Low-power photomicrographs of biocytin-labeled MCs in WT (*A*) and reeler slices (*B*, *C*). (*D–F*) High-power micrographs of the same neurons. Note the characteristic complex spines on the proximal dendrites (arrows). (*G–I*) Neurolucida reconstruction of biocytin-filled WT (*G*) and reeler MCs (*H*, *I*). While all dendrites (in black) of the WT MCs are confined to the hilus (hil), many dendrites of reeler MCs extend beyond the boundary of the GC layer–hilus area (gcl–hilus, dashed line) into the molecular layer (ml). The axons (in gray) only have a limited extent within the slices. (*J*, *K*) Bar charts of the total dendritic length (*J*) and proportion of the dendrites (percentage of total length) extending into the ml (*K*) of 13 WT and 9 reeler MCs. Open circles superimposed on the bars represent the individual cells. (*L*, *M*) The number of dendritic segments (*L*) and their summed length (*M*) plotted against branch order. Significant differences between the WT and reeler groups are indicated by asterisks ($*P < 0.05$; $**P < 0.005$).

from the electrophysiological data obtained in whole-cell patch-clamp recordings (Fig. 4). Responses elicited by hyper- and depolarizing current pulses in MCs from both WT and reeler slices revealed characteristic intrinsic properties (Fig. 4*A*,*B*) distinct from other neuronal types (Lübke et al. 1998; Kerr and Capogna 2007; Larimer and Strowbridge 2008). No significant differences between WT and reeler groups were detected in terms of passive membrane properties such as the resting membrane potential, input resistance, and apparent membrane time constant (Table 1). In contrast, analysis of active properties revealed subtle differences in the AP waveform (Fig. 4*C*,*D*). In particular, the rate of AP rise was significantly faster and the AHP larger in the reeler mutant than in WT littermates (Table 1). These changes in the AP waveform may reflect an increased density of voltage-gated sodium and potassium channels in the perisomatic compartment of reeler MCs (Bean 2007). In contrast, other parameters including the AP threshold and firing frequency were comparable between the groups (Table 1).

We have also noted differences in spontaneous synaptic events in reeler MCs. To evaluate these differences, we determined the frequency and amplitude of spontaneous EPSCs in traces recorded in VC mode. We found that the frequency of the EPSCs was significantly reduced in reeler MCs (6.7 ± 0.6 Hz, 43 cells) in comparison to WT (13.7 ± 1.7 Hz, 21 cells; $P = 0.001$). In contrast, the mean amplitude of the

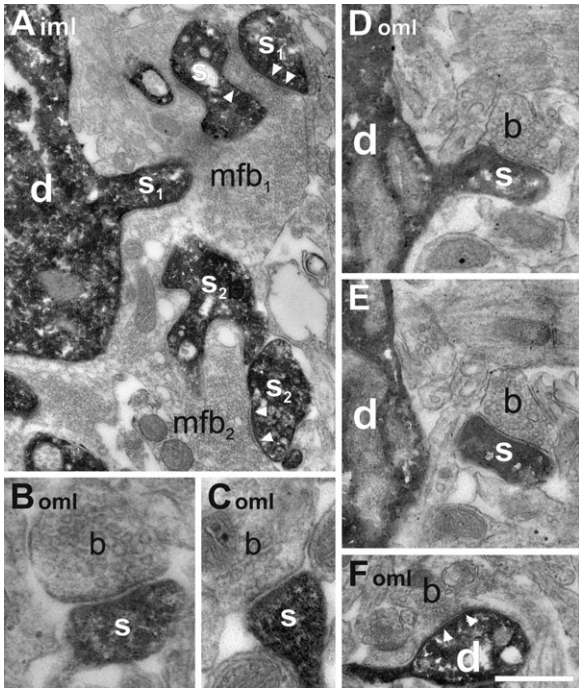

Figure 3. Ectopic reeler MC dendrites receive synaptic inputs in the molecular layer. (*A*) Electron photomicrograph illustrates the thick proximal dendrite (d) and 2 complex spines (s1, s2) of a biocytin-labeled MC located in the inner molecular layer (iml). Two mossy fiber boutons (mfb1, mfb2) engulf the spines and form synaptic contacts (arrowheads). (*B*, *C*) Distal dendritic spines (s) of the same MC receive synaptic inputs from small unlabeled boutons (b) in the outer molecular layer (oml). (*D*, *E*) Serial electron micrographs show a spine (s) on a distal dendrite (d) of another biocytin-labeled MC contacted by a small bouton (b) in the oml. The soma of this MC was located in the central hilus. (*F*) Synaptic contact formed by an unlabeled bouton (b) onto a biocytin-labeled MC dendritic shaft in the molecular layer. Scale bars: *A*—0.63 μm, *B*, *C*—0.2 μm, *D*, *E*—0.5 μm, *F*—0.6 μm.

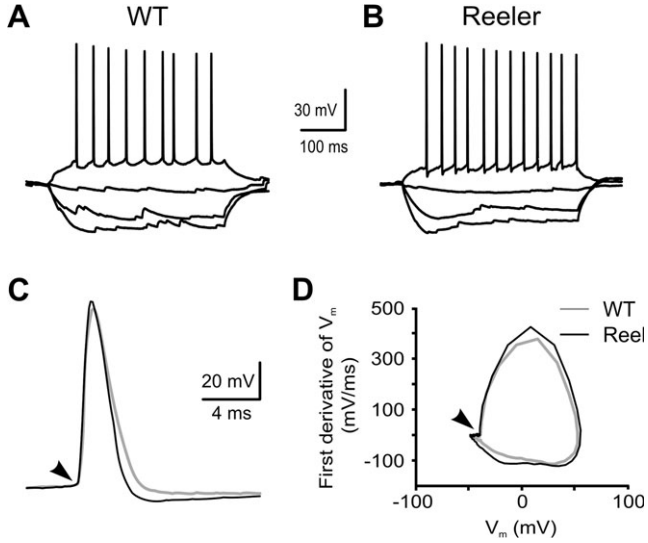

Figure 4. Active properties of reeler MCs are altered. (*A*, *B*) Responses of WT (*A*) and reeler MCs (*B*) to a series of hyperpolarizing and depolarizing current pulses (-200 to 100 pA, 200 ms). (*C*) Superimposed single APs from a WT (gray) and a reeler MC (black). The AP trajectories were aligned at the threshold crossing (arrowhead). Note the larger amplitude and shorter duration of the AP in the reeler. (*D*) In the phase plot, the first derivative of the AP waveform (dV_m/dt) is plotted against the corresponding membrane potential (V_m) from the WT (gray) and the reeler MC (black). The larger positive and negative peak values of the derivative indicate faster rates of AP rise and decay, respectively, in the reeler MC. Arrowhead indicates the point of threshold crossing.

spontaneous EPSCs was similar in reeler (82.6 ± 4.8 pA) and WT MCs (88.7 ± 7.0 pA; $P = 0.26$).

Reeler MCs Receive Monosynaptic Excitatory Input from the PP

The presence of synaptic contacts in the outer molecular layer on the distal dendritic spines of reeler MCs indicated that these cells may receive substantial excitatory input directly from the PP. To test this hypothesis, we stimulated the PP and recorded the synaptic responses in WT and reeler MCs in VC mode (Fig. 5). To monitor the activation of the GC population, EC field potentials were simultaneously recorded at the crest of the GC layer. The stimulus intensity was set below the threshold for generating an EC PS (mean stimulus intensity was 80 ± 6 μA for WT and 63 ± 6 μA for reeler). However, when pairs of stimuli were applied in short succession (50 ms), paired-pulse facilitation (PPF) resulted in a PS on the second response, indicating the synchronous activation of a subset of GCs in both WT and reeler DG (Fig. 5*A*,*B*, upper traces).

In the absence of a PS, the synaptic response to the first stimulus was dominated by a compound IPSC in both WT and reeler MCs (Fig. 5*A*,*B*, lower traces). While the mean onset latency (2.6 ± 0.1 ms, 19 WT MCs vs. 2.5 ± 0.1 ms, 28 reeler MCs) and the half-duration (8.3 ± 0.9 ms vs. 7.6 ± 0.7 ms) of the IPSC were similar, the peak amplitude of the IPSC was larger in reeler than in WT MCs (120 ± 14 pA in WT vs. 273 ± 32 pA in reeler MCs, $P < 0.001$).

In response to the second pulse, which elicited a small PS (mean amplitude in WT 0.34 ± 0.08 mV, in reeler 0.12 ± 0.01 mV), long-latency EPSCs were superimposed on the compound IPSC (Fig. 5*A*,*B*, lower traces, Fig. 5*C*, black traces). The latency of the EPSC onset after the stimulus was 5.5 ± 0.2 ms in WT and 5.6 ± 0.3 ms in reeler MCs. These EPSCs occurred consistently after the PS (relative latency: 2.3 ± 0.2 ms in WT MCs and 2.9 ± 0.3 ms in reeler, Fig. 5*D*, left), indicating that these were disynaptic EPSCs, conceivably mediated by GCs. Indeed, whole-cell patch-clamp recordings from GCs showed that these neurons received monosynaptic EPSCs and discharged with short latency in response to the PP input in both WT and reeler slices (see Supplementary Fig. 1). The amplitude of the disynaptic EPSCs in the averaged responses was large in WT (251 ± 51 pA), but significantly smaller in reeler MCs (97 ± 23 pA, $P = 0.009$, Fig. 5*D*, right).

In addition to the disynaptic EPSCs, short-latency EPSCs could also be identified in the majority of reeler MCs (22 of 28 cells; Fig. 5*B*, lower traces, Fig. 5*C*, right). The onset of these EPSCs had a mean latency of 2.1 ± 0.2 ms from the stimulus and preceded the PS (relative latency: –0.7 ± 0.1 ms; Fig. 5*D*, left). The onset latency of these EPSCs was comparable to that of the EPSCs recorded in WT and reeler GCs (Supplementary Fig. 1*A*). Therefore, these EPSCs were of monosynaptic origin, consistent with a direct synaptic input from the PP onto MCs in reeler. The amplitude of the EPSCs was small in the first response (23 ± 7 pA), but larger in the second response (82 ± 21 pA, $P < 0.001$; Fig. 5*D*, right), reflecting PPF at this monosynaptic input. No monosynaptic EPSCs were observed in any of the WT MCs recorded in these experiments.

In order to isolate monosynaptic EPSCs in reeler MCs, we recorded synaptic responses to PP stimulation in the molecular

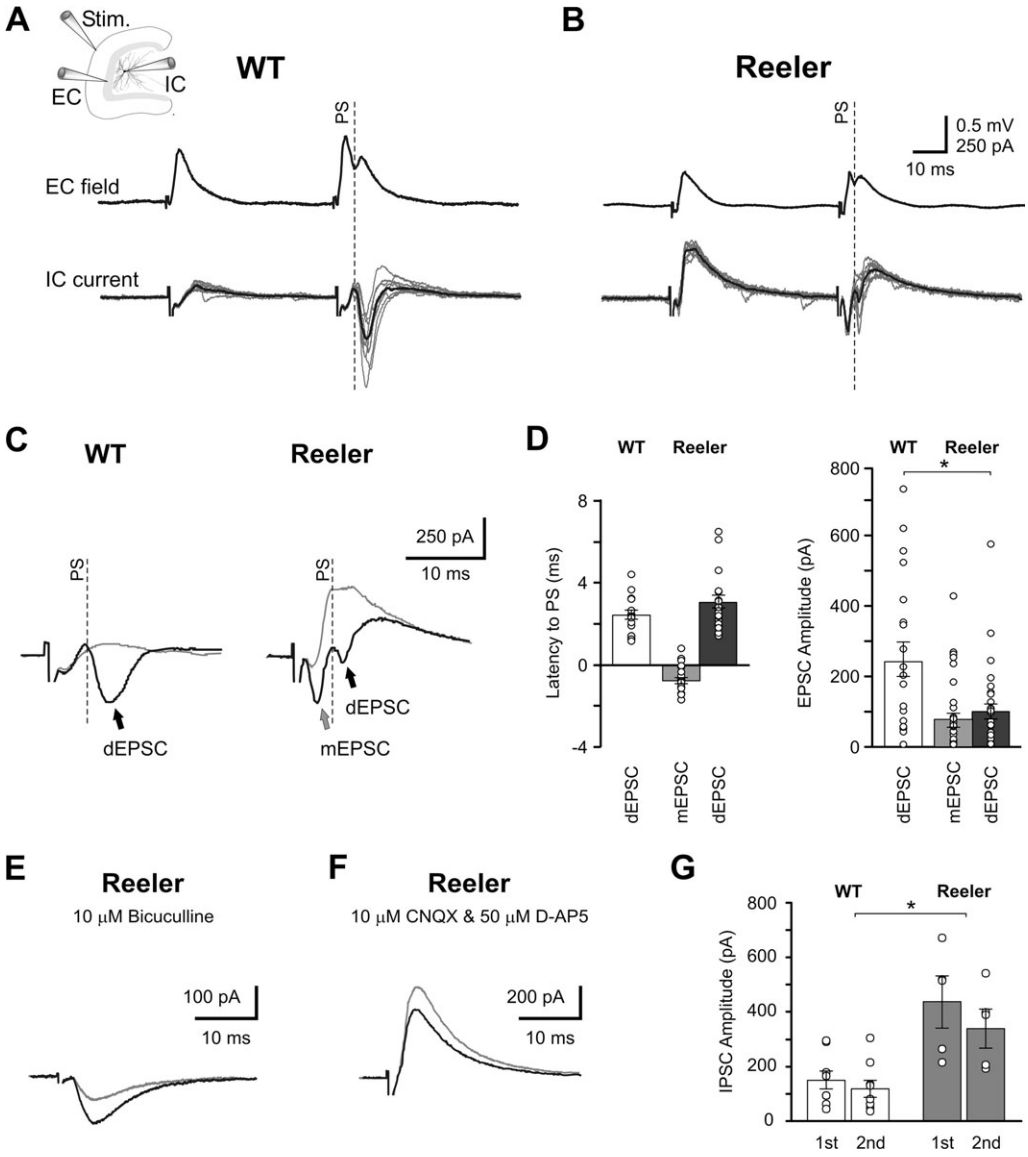

Figure 5. Aberrant excitation and increased inhibition in reeler MCs. (*A*) Simultaneous EC field potentials recorded in the GC layer (upper trace, average of 9 responses) and whole-cell VC recordings from a WT MC (lower traces, averaged response in black superimposed on the individual traces in gray). Synaptic responses were elicited by low intensity (40 μA, 0.1 ms) paired stimuli applied to the PP in the outer molecular layer (see inset for the arrangement of the stimulating and the recording electrodes). Vertical dashed lines indicate the timing of the EC PS that was elicited by the second stimulus. (*B*) Simultaneous EC (average of 9 traces) and intracellular recording of synaptic responses (stimulus: 40 μA, 0.1 ms) in a reeler slice. (*C*) Superimposed averages of typical intracellular synaptic responses to the first (gray lines) and second stimulus (black lines) in the WT (left) and reeler MC (right). While the first responses were dominated by a compound IPSC, the second responses were characterized by long-latency, disynaptic EPSCs (dEPSCs, black arrows) that become obvious in the presence of a PS in the EC recording, thus indicating the discharge of a larger set of GCs. In reeler, a short-latency, monosynaptic EPSC (mEPSC, gray arrow) was also observed. The vertical dashed line indicates the timing of the EC PS separating the mEPSC and the dESPCs. (*D*) Bar charts show the relative onset latencies measured from the PS (left) and amplitudes (right) of the mEPSC (gray) and dEPSC (black) at the second responses in 19 WT and 28 reeler MCs. Open circles superimposed on the bars represent the individual cells. Asterisk indicates significant difference ($P = 0.009$). (*E*) Superimposed averages of mEPSCs at the first (gray line) and second response (black line) recorded from a reeler MC in the presence of 10 μM bicuculline. (*F*) Monosynaptic IPSCs recorded from a reeler MC in the presence of 10 μM CNQX and 50 μM D-AP5. Note the paired-pulse depression of the IPSCs. (*G*) Bar chart of the amplitudes of pharmacologically isolated monosynaptic IPSCs in WT (9 cells) and reeler MCs (5 cells). Open circles superimposed on the bars represent the individual cells. The IPSCs are substantially larger in reeler than in WT.

layer after the $GABA_A$ receptor blocker bicuculline (10 μM) was applied to the bath, and stimulus intensity was lowered (20–40 μA) to avoid reverberating excitation in the disinhibited network. Under these conditions, short latency (2.4 ± 0.2 ms) monosynaptic EPSCs were observed in 5 of 6 reeler MCs tested (Fig. 5). The peak amplitude and decay time constants of these monosynaptic EPSCs were 37 ± 12 pA and 5.6 ± 1.7 ms. In response to paired stimuli, the EPSCs showed a strong facilitation with a mean amplitude of 79 ± 30 pA at the second response.

Visualization of the recorded cells revealed differences in the excitatory synaptic inputs dependent on the location of the cell (Supplementary Fig. 2*A*). While the synaptic responses in all MCs with somata in the molecular layer (11 cells) consisted of both monosynaptic and disynaptic EPSCs, the responses in cells with somata located in the hilus were heterogeneous: 6 of 17 cells showed no discernible monosynaptic EPSCs and 6 other cells showed no disynaptic EPSCs. The mean amplitude of monosynaptic EPSCs was substantially larger (120 ± 41 pA) in cells in the molecular layer that had

higher proportion of the dendrites extending into this layer (see above) than in hilar cells (57 ± 22 pA, $P = 0.03$). There was no significant difference between the 2 groups in the amplitude of the disynaptic EPSCs (86 ± 20 pA in molecular layer MCs vs. 104 ± 37 pA in hilar MCs, $P = 0.57$). Analysis of the compound IPSCs did not reveal a correlation between somal location and amplitude either (Supplementary Fig. 2*B*).

Taken together, these results show that reeler MCs receive aberrant monosynaptic excitatory input from the PP, whereas transmission through the normal disynaptic input via GCs appears to be reduced.

Enhanced Monosynaptic Inhibition in Reeler MCs

The larger amplitude of compound IPSCs indicates an increased inhibitory input onto reeler MCs. To further investigate this aspect, we next recorded pharmacologically isolated monosynatic IPSCs in response to PP stimulation (intensity: 88 ± 9 μA for WT and 74 ± 8 μA for reeler) after washing in blockers of fast glutamatergic transmission, CNQX (10 μM) and D-AP5 (50 μM, Fig. 5*G*,*F*). In WT MCs (9 cells), the monosynaptic IPSCs had an onset latency of 2.6 ± 0.1 ms, a decay time constant of 7.3 ± 0.7 ms, and a peak amplitude of 150 ± 33 pA. In reeler MCs, the time course of the IPSCs was comparable (latency: 2.2 ± 0.3 ms, decay time constant: 7.9 ± 0.8 ms), whereas the peak amplitude was markedly larger (436 ± 96 pA, 5 cells, $P = 0.01$). In both WT and reeler MCs, monosynaptic IPSCs showed a depression of ~20% in response to the paired stimuli (IPSC amplitude at the second stimulus: 120 ± 32 pA in WT and 344 ± 73 pA in reeler MCs). These data, therefore, corroborate that reeler MCs receive a stronger inhibitory input than WT MCs.

Reeler MCs Are Activated with Monosynaptic Latencies

How do the changes in synaptic input influence the activation of reeler MCs? To address this question, we have recorded voltage responses of the neurons to the paired EC stimuli in CC mode (Fig. 6). In order to enhance the activation of the neurons, we increased stimulus intensities to values, which elicited a PS in the EC field recording already at the first response. In response to this high stimulus intensity, 5 of 16 tested WT MCs fired APs at the first and 13 cells fired at the second response (Fig. 6*A*), conceivably reflecting facilitation of excitatory transmission and depression of inhibition in the underlying circuit (Lysetskiy et al. 2005; Kerr and Capogna 2007). Reeler MCs also showed PPF, with 9 of 24 tested cells firing an AP in response to the first and 15 cells activated by the second stimulus (Fig. 6*C*,*E*).

Next, we analyzed the timing and reliability of AP generation in the active neurons. In WT MCs, APs were elicited with long latency after the stimuli. The APs always occurred after the PS that was recorded from the GC layer (Fig. 6*A*), indicating that MCs were disynaptically activated via GCs (Buckmaster et al. 1993). AP initiation showed several differences between the first and the second responses to the paired stimulus. First, the mean latency of APs was reduced from the first to the second response (9.1 ± 0.8 ms vs. 6.6 ± 0.4 ms, measured from stimulus onset). Second, the reduced latency was accompanied by an increase in temporal precision, reflected by the steeper rise in the cumulative discharge probability curve at the second response (Fig. 6*B*). Indeed, the standard deviation (SD) of the AP latencies reflected a broad temporal window at the first response (1.8 ± 0.6 ms), but a markedly shorter window at the second (0.6 ± 0.1 ms, $P = 0.0016$). Finally, the mean probability of eliciting an AP was low after the first stimulus (0.13 ± 0.07), but significantly higher after the second stimulus (0.73 ± 0.09, $P < 0.001$, Fig. 6*B*). These differences in the timing and reliability of AP initiation in MCs correlated well with the

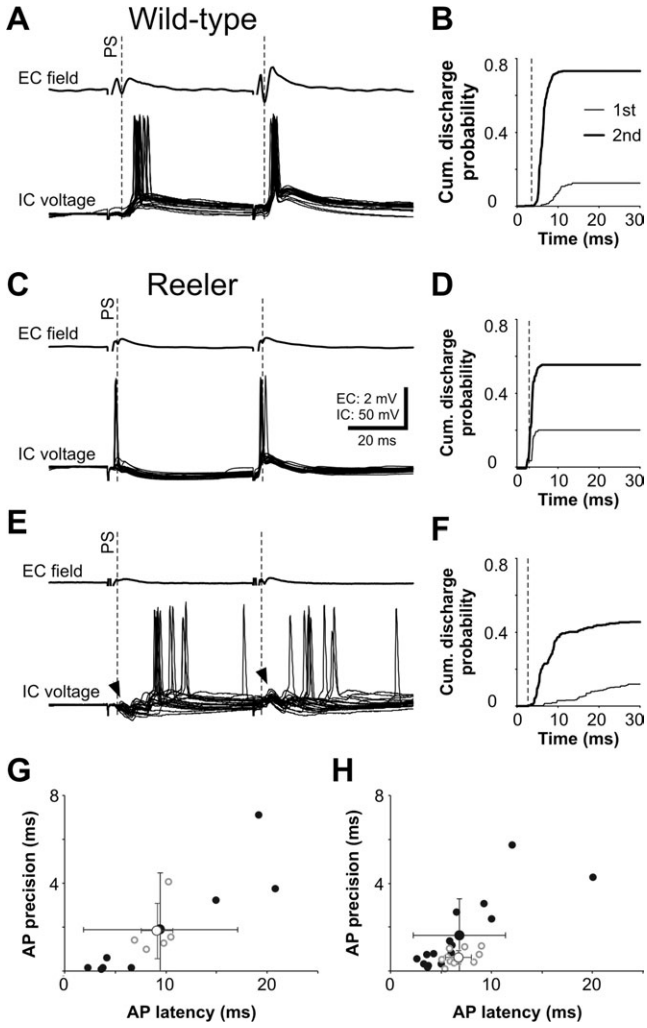

Figure 6. Altered timing of AP initiation in reeler MCs in response to synaptic activation through the PP. (*A*) Extracellular field potential recorded in the GC layer (upper trace, average of 20 responses) and intracellular voltage recording from a WT MC (20 superimposed individual traces). WT MCs showed a uniform activation pattern and discharge with disynaptic latencies in response to high intensity PP stimulation. APs always occurred with disynaptic latencies after the EC PS (vertical dashed lines). (*B*) The cumulative probability curves of AP generation (averaged curves from 13 WT MCs) show that PPF led to faster, stronger, and temporally precise activation of MCs at the second response (thick line). The dashed line indicates the time of the PS. (*C*–*F*) Similar plots for reeler MCs illustrate altered and heterogeneous activation patterns. In 7 of the 15 reeler MCs, APs occurred with short latency before the EC PS, indicating that they were initiated by the monosynaptic excitatory inputs (*C*). The averaged cumulative probability plots show that activation was precisely timed at both the first and the second response in these cells (*D*). In 8 reeler MCs, APs were generated with long latency and reduced precision (*E*, *F*). Monosynaptic EPSPs (arrows in *E*) could also be observed in some of these cells. (*G*, *H*) Precision (measured as the SD of individual AP latencies) is plotted against the mean latency of AP discharge for each neuron at the first (*G*) and the second responses (*H*). While WT MCs (open circles) form a homogeneous cluster around their group means (large open circles with error bars indicating SDs), reeler cells (filled circles) show broad scatter along both axes, reflecting the large heterogeneity in the latency and temporal precision of synaptic activation in these neurons.

changes in latency and amplitude of the EC PS. The mean latency was 5.0 ± 0.4 ms and the amplitude 0.5 ± 0.1 mV at the first response, whereas the latency was significantly shorter (4.0 ± 0.2 ms, $P < 0.001$) and the amplitude larger (1.6 ± 0.3 mV, $P < 0.001$) at the second response (Fig. 6*A*, upper trace). These data therefore show that WT MCs are discharged disynaptically, and their enhanced activation occurring in response to the second stimulus is dependent on the faster and stronger recruitment of dentate GCs. However, it is plausible that the large extent of facilitation in the discharge probability is also dependent on the robust PPF observed at the mossy fiber-MC synapses (Lysetskiy et al. 2005; Kerr and Capogna 2007).

In contrast to the uniform responses observed in WT MCs, reeler MCs showed a high degree of heterogeneity in their activation pattern (Fig. 6*C–F*). Although the mean AP latencies (9.4 ± 2.9 ms at the first response and 6.7 ± 1.2 ms at the second response) were comparable to those in WT MCs, the distribution of the values for the individual cells was markedly broader (*F*-test, $P = 0.008$ for first response, $P < 0.001$ for second response). When the mean AP latencies for the individual cell were plotted against the respective SDs, WT MCs clustered closely around the group averages (Fig. 6*G,H*, open circles), whereas the points representing the reeler MCs spread broadly along both axes (Fig. 6*G,H*, filled circles). Reeler cells could be split into 2 sets: in one set, the neurons discharged with short latencies and precise timing before or at the same time as the PS; in the other set, they fired with long and variable latencies after the PS. While the discharge pattern was stable for the majority of reeler MCs over the stimulus intensity range tested, 3 cells switched from long-latency to short-latency activation as the stimulus intensity was increased. Additionally, one cell fired long-latency APs at the first response and short-latency APs at the second response. AP latency did not show a clear correlation with the position of the cells (Supplementary Fig. 2*C*). This could be explained by the high variability in the excitatory and inhibitory synaptic inputs observed in the VC recordings.

A short-latency discharge pattern was observed in half of the active reeler MCs (7 of 15, 47%; Fig. 6*C*). Four of these cells fired APs with short latencies at the first response, while all 7 fired such APs at the second response. The mean AP latency in these cells was significantly shorter than that in WT MCs (3.5 ± 0.5 ms, $P = 0.02$ at the first and 3.6 ± 0.3 ms, $P < 0.001$ at the second response). APs occurred before or at the same time as the EC PS (mean latency of the PS: 3.7 ± 0.4 ms at the first and 3.4 ± 0.4 ms at the second response; Fig. 6*C*, upper trace), indicating that they were triggered by monosynaptic inputs. Consistent with a monosynaptic activation, APs were generated with precise timing within a narrow temporal window in response to both stimuli (SD of the AP latencies was 0.2 ± 0.1 ms at the first response and 0.4 ± 0.1 ms at the second). Finally, the discharge probability showed facilitation from the first to the second stimulus (0.22 ± 0.09 vs. 0.56 ± 0.15, $P = 0.016$, Fig. 6*D*).

A long-latency discharge pattern was observed at high stimulus intensities in 8 of the reeler MCs (53%; Fig. 6*E*). Similar to the previous group, only 4 cells fired at the first response and all 8 at the second. The latency of the APs was longer, but not significantly different than in WT cells and had a mean value of 15.4 ± 3.7 ms ($n = 4$) at the first and 9.3 ± 1.8 ms at the second response. The EC PS always preceded the APs (mean latency of the PS: 3.3 ± 0.3 ms at the first and 3.3 ± 0.2 ms at the second response; Fig. 6*E*, upper trace), indicating that these cells were driven by disynaptic and polysynaptic excitatory inputs. The contribution of disynaptic and polysynaptic inputs to the activation of the cells was also reflected by the low precision of APs initiated over a broad temporal window (SD of the AP latencies was 3.5 ± 1.7 for the first response and 2.6 ± 0.6 ms for second). Although the discharge probability in these cells was comparable to those observed at the first stimulus in WT MCs (0.09 ± 0.05), it was lower after the second stimulus (0.46 ± 0.09, $P = 0.046$).

In summary, consistent with the aberrant monosynaptic excitatory input, a large subset of reeler MCs discharged with monosynaptic latencies in response to PP input. However, at the population level, synaptic activation of reeler MCs showed increased heterogeneity in comparison to the uniform disynaptic discharge pattern of WT MCs.

Discussion

Our study has revealed that altered layering in the hippocampus is associated with marked changes in the morphology, connectivity, and synaptic activation of MCs in reeler mice. Aberrant excitatory input from the PP targets MC dendrites extending into the molecular layer and activates many of these cells with short, monosynaptic latencies. At the population level, reeler MCs show a high level of heterogeneity in their synaptic input and activation patterns. The altered timing of AP discharge leads to asynchronous activation of MCs in the reeler dentate-hilar network. Together, these results provide insights into the functional importance of cortical layering.

Altered Localization and Morphology of Reeler MCs

In reeler mice, neuronal migration defects result in the altered lamination of cortical structures (Falconer 1951). In the DG, GCs lose their alignment and orientation, leading to dispersion of the normally densely packed somatic layer (Caviness and Rakic 1978; Stanfield and Cowan 1979; Drakew et al. 2002; Förster et al. 2006). Our study reveals that the position and morphology of MCs are also altered. In WT mice, the soma and dendrites are confined to the hilus (Ribak et al. 1985; Frotscher et al. 1991; Buckmaster et al. 1993; but see Scharfman 1991), whereas in reeler, MC somata are scattered throughout the hilus and inner molecular layer. Moreover, regardless of somal location, dendrites consistently extend into the molecular layer, the termination zone of the PP. Intriguingly, while complexity of the branching pattern is reduced, the total dendritic length of the cells is unchanged. It remains to be established whether changes in the dendritic arbor are a consequence of the altered lamination of the surrounding structure or a direct result of the lack of Reelin during development (Niu et al. 2004; Chai et al. 2009).

In contrast to the overt anatomical changes, less prominent differences were detected in the physiological properties of reeler MCs, with passive intrinsic properties remaining unaffected. Such properties, particularly the input resistance and membrane capacitance, are explored by somatic CC recording and determined primarily by membrane parameters and structure of the somatodendritic compartment (Jack 1975; Spruston et al. 1994). These data therefore concur with the unaltered somal size and total dendritic length. In contrast, active properties are changed in a subtle, but consistent manner. Plausibly, the increased rate of AP rise and AHP amplitude indicates a higher density of voltage-gated Na^+ and

K^+ channels in compartments close to the somatic recording site (Bean 2007). Interestingly, the threshold of APs remains unchanged, suggesting that the properties of Na channels are largely preserved. Although the cause and functional relevance of these changes need further investigation, the higher sodium channel density may contribute to an enhanced amplification of excitatory inputs (Stuart and Sakmann 1995; González-Burgos and Barrionuevo 2001).

Changes in the Synaptic Input on to MCs in the Reeler Dentate-Hilar Network

The presence of reeler MC dendrites in the outer molecular layer indicates that they receive substantial direct excitatory input from the PP, as the majority of presynaptic elements in this layer belong to the PP (Borrell, Del Rio, et al. 1999). Indeed, our electron microscopic investigation provides evidence for existing synapses on these ectopic dendrites. Moreover, the high occurrence of monosynaptic EPSCs elicited in reeler MCs by stimulation within the outer molecular layer further supports this scenario. However, we cannot exclude that in some cases ectopic mossy fibers might have contributed to these evoked responses.

Aberrant synaptic contacts have previously been found in the cerebellar cortex of reeler mice (Sotelo 1990). However, in the neocortex and hippocampus, the majority of previous electrophysiological and anatomical studies suggest that the specificity of synaptic connections between pre- and postsynaptic elements is maintained in reeler mice (Bliss and Chung 1974; Caviness and Frost 1983; Deller et al. 1999; Drakew et al. 2002; Gebhardt et al. 2002; Pascual et al. 2004). Although it was recently proposed that the overlap of mossy fibers and GC dendrites may lead to abnormal synapses in the hilus (Patrylo et al. 2006), no direct evidence for this has been provided. Our results now demonstrate that the spatial overlap of heterologous pre- and postsynaptic elements, which are segregated in the properly layered cortex, leads to the formation of aberrant synapses in the reeler hippocampus.

The physiological data further indicate that the disrupted lamination in the reeler hippocampus results in a changed balance of excitation and inhibition in MCs. The reduced excitatory transmission through the DG disynaptic pathway could be explained by the decreased overlap of natural pre- and postsynaptic partners, which in turn leads to sparser connectivity. The dispersion and radial disorientation of GCs mean that a lower portion of their dendrites is localized within the PP termination zone in the reeler mutant (Drakew et al. 2002). Similarly, as shown in this study, the proportion of MC dendrites overlapping with mossy fibers in the hilus is also reduced. Reelin promotes the branching of PP axons (Borrell, Del Rio, et al. 1999) and the development of postsynaptic spines (Liu et al. 2001; Niu et al. 2008); therefore, the lack of this effect in reeler mice may exacerbate the reduced connectivity.

While these anatomical anomalies of reeler MCs can adequately explain the changes observed in excitatory synaptic transmission, functional changes could also contribute. Reelin enhances glutamatergic transmission and synaptic plasticity by influencing α-amino-3-hydroxyl-5-methyl-4-isoxazole-propionat and N-methyl-D-aspartate receptor function (Beffert et al. 2005; Qui et al. 2006). Therefore, the weaker disynaptic excitatory input to MCs may also reflect reduced glutamatergic transmission in these mutant mice.

Mechanisms underlying the enhanced inhibition in reeler mice (present results; Ishida et al. 1994) are less clear. Little is known about changes in the GABAergic system in reeler mice, but there is compelling evidence for GABAergic hypofunction in heterozygous mice (Liu et al. 2001; Carboni et al. 2004). However, this hypofunction involves the GAD67 isoform of the GABA synthesizing enzyme, whereas the dominant GAD65 isoform is unaffected (Liu et al. 2001). Furthermore, cell counts suggest that no major cell loss occurs in the cortex of heterozygous and homozygous reeler mice (Coulin et al. 2001; Liu et al. 2001). On the contrary, certain types of interneurons are increased in number (Coulin et al. 2001). Therefore, it is not possible to predict the net change in inhibition in the reeler hippocampus. An explanation for the observed enhanced inhibition in MCs could be that they receive input from a larger pool of interneurons. In WT MCs, feedforward inhibition is conspicuously weak (Scharfman and Schwartzkroin 1988; Buckmaster et al. 1993); MCs are preferentially connected to hilar interneurons by feedback loops (Larimer and Strowbridge 2008). Although these connections are likely to be preserved in reeler, the ectopic MC dendrites provide the substrate for additional input from DG interneurons (Han et al. 1993; Scharfman 1995). Conversely, an altered, broader distribution of interneuron axons, such as DG basket cells, may enable the formation of heterologous inhibitory synapses onto reeler MCs.

It has been proposed that GC dispersion may lead to abnormal, proconvulsive glutamatergic connectivity in the hilus (Patrylo et al. 2006; Patrylo and Willingham 2007). Consistent with this proposal, polysynaptic excitatory responses were observed in some reeler MCs reflecting reverberating activity in the network. However, the activation of MCs was not enhanced, indicating that the aberrant connectivity is weak and efficiently counterbalanced by the enhanced inhibition. Thus, our results suggest that excitability of the dentate-hilar network is not increased; epileptiform activity can develop only when inhibition is compromised (Patrylo et al. 2006).

Altered Timing and Heterogeneity of Synaptic Activation in the Reeler Network

As expected from the modified inputs, the synaptic activation of reeler MCs is also altered. In WT MCs, APs are uniformly generated, with disynaptic latencies in response to PP stimulation (Buckmaster et al. 1993; present data). Thus, activation of WT MCs is mediated by GCs (Lysetskiy et al. 2005). In contrast, many reeler MCs discharge with monosynaptic latencies, in good agreement with a direct PP input to these cells, while others discharge with long, disynaptic and polysynaptic latencies and low temporal precision. These differences in the activation of reeler MCs are consistent with the high level of heterogeneity in their morphology and synaptic inputs. At the population level, this heterogeneous timing will translate into asynchronous activity of the neurons and compromise network functions in reeler mice.

In summary, our study reveals that disrupted cortical lamination leads to altered timing and asynchrony of neuronal discharge. It has been proposed that proper laminar organization is important for optimal wiring, minimizing the costs involved in the assembly and maintenance of the circuit, while maximizing functionality (Chklovskii 2004; Wen and Chklovskii et al. 2008). Indeed, altered lamination in the reeler DG disrupts the normal connectivity and leads to the development

of aberrant synapses. Importantly, individual neurons are not uniformly affected; rather, their synaptic inputs become heterogeneous and their activation asynchronous. A temporally precise discharge of neurons is an essential feature of cortical activity that underlies synaptic plasticity and the emergence of neuronal assemblies (Dan and Poo 2004; Fries et al. 2007; Klausberger and Somogyi 2008). Therefore, the present results provide a basis for understanding the neurological phenotype associated with the lack of Reelin in mice as well as human patients and have implications for information processing in the intact, layered cortical structure.

Supplementary Material

Supplementary material can be found at: http://www.cercor.oxfordjournals.org/.

Funding

Deutsche Forschungsgemeinschaft (Sonderforschungsbereich 505 and Transregional 3); Bundesministerium für Bildung und Forschung (01GQ0420); Excellence Initiative of the German Federal and State Governments (GSC-4, Spemann Graduate School).

Notes

We thank S. Nestel, U. Nöller, and A. Schneider for their excellent technical assistance. We also thank Drs M. Bartos, S.R. Cobb, T. Deller, U. Egert, and J. Staiger for their valuable comments on an early version of the manuscript. *Conflict of Interest*: None declared.

References

Amaral DG. 1978. A Golgi study of cell types in the hilar region of the hippocampus in the rat. J Comp Neurol. 182:851–914.

Amaral DG, Witter MP. 1989. The three-dimensional organization of the hippocampal formation: a review of anatomical data. Neuroscience. 31:571–591.

Bean BP. 2007. The action potential in mammalian central neurons. Nat Rev Neurosci. 8:451–465.

Beffert U, Weeber EJ, Durudas A, Qiu S, Masiulis I, Sweatt JD, Li WP, Adelmann G, Frotscher M, Hammer RE, et al. 2005. Modulation of synaptic plasticity and memory by Reelin involves differential splicing of the lipoprotein receptor Apoer2. Neuron. 47:567–579.

Blasco-Ibanez JM, Freund TF. 1997. Distribution, ultrastructure, and connectivity of calretinin-immunoreactive mossy cells of the mouse dentate gyrus. Hippocampus. 7:307–320.

Bliss TV, Chung SH. 1974. An electrophysiological study of the hippocampus of the '*reeler*' mutant mouse. Nature. 252:153–155.

Borrell V, Del Rio JA, Alcantara S, Derer M, Martinez A, D'Arcangelo G, Nakajima K, Mikoshiba K, Derer P, Curran T, et al. 1999. Reelin regulates the development and synaptogenesis of the layer-specific entorhino-hippocampal connections. J Neurosci. 19:1345–1358.

Borrell V, Ruiz M, Del Rio JA, Soriano E. 1999. Development of commissural connections in the hippocampus of *reeler* mice: evidence of an inhibitory influence of Cajal-Retzius cells. Exp Neurol. 156:268–282.

Buckmaster PS, Schwartzkroin PA. 1994. Hippocampal mossy cell function: a speculative view. Hippocampus. 4:393–402.

Buckmaster PS, Strowbridge BW, Schwartzkroin PA. 1993. A comparison of rat hippocampal mossy cells and CA3c pyramidal cells. J Neurophysiol. 70:1281–1299.

Buckmaster PS, Wenzel HJ, Kunkel DD, Schwartzkroin PA. 1996. Axon arbors and synaptic connections of hippocampal mossy cells in the rat in vivo. J Comp Neurol. 366:271–292.

Burgess N, Maguire EA, O'Keefe J. 2002. The human hippocampus and spatial and episodic memory. Neuron. 35:625–641.

Carboni G, Tueting P, Tremolizzo L, Sugaya I, Davis J, Costa E, Guidotti A. 2004. Enhanced dizocilpine efficacy in heterozygous *reeler* mice relates to GABA turnover downregulation. Neuropharmacology. 46:1070–1081.

Caviness VS, Jr, Frost DO. 1983. Thalamocortical projections in the *reeler* mutant mouse. J Comp Neurol. 219:182–202.

Caviness VS, Jr, Rakic P. 1978. Mechanisms of cortical development: a view from mutations in mice. Annu Rev Neurosci. 1:297–326.

Chai X, Förster E, Zhao S, Bock HH, Frotscher M. 2009. Reelin stabilizes the actin cytoskeleton of neuronal processes by inducing n-cofilin phosphorylation at serine3. J Neurosci. 29:288–299.

Chklovskii DB. 2004. Synaptic connectivity and neuronal morphology: two sides of the same coin. Neuron. 43:609–617.

Coulin C, Drakew A, Frotscher M, Deller T. 2001. Stereological estimates of total neuron numbers in the hippocampus of adult *reeler* mutant mice: evidence for an increased survival of Cajal-Retzius cells. J Comp Neurol. 439:19–31.

Dan Y, Poo MM. 2004. Spike timing-dependent plasticity of neural circuits. Neuron. 44:23–30.

D'Arcangelo G, Miao GG, Chen SC, Soares HD, Morgan JI, Curran T. 1995. A protein related to extracellular matrix proteins deleted in the mouse mutant. Nature. 374:719–723.

Deller T, Drakew A, Frotscher M. 1999. Different primary target cells are important for fiber lamination in the fascia dentata: a lesson from *reeler* mutant mice. Exp Neurol. 156:239–253.

Drakew A, Deller T, Heimrich B, Gebhardt C, Del Turco D, Tielsch A, Förster E, Herz J, Frotscher M. 2002. Dentate granule cells in *reeler* mutants and VLDLR and ApoER2 knockout mice. Exp Neurol. 176:12–24.

Falconer DS. 1951. 2 new mutants, trembler and *reeler*, with neurological actions in the house mouse (Mus-Musculus L). J Genet. 50:192–201.

Förster E, Zhao S, Frotscher M. 2006. Laminating the hippocampus. Nat Rev Neurosci. 7:259–267.

Fries P, Nikolic D, Singer W. 2007. The gamma cycle. Trends Neurosci. 30:309–316.

Frotscher M, Seress L, Schwerdtfeger WK, Buhl E. 1991. The mossy cells of the fascia dentata: a comparative study of their fine structure and synaptic connections in rodents and primates. J Comp Neurol. 312:145–163.

Frotscher M, Zhao S, Förster E. 2007. Development of cell and fiber layers in the dentate gyrus. Prog Brain Res. 163:133–142.

Gebhardt C, Del Turco D, Drakew A, Tielsch A, Herz J, Frotscher M, Deller T. 2002. Abnormal positioning of granule cells alters afferent fiber distribution in the mouse fascia dentata: morphologic evidence from *reeler*, apolipoprotein E receptor 2-, and very low density lipoprotein receptor knockout mice. J Comp Neurol. 445:278–292.

González-Burgos G, Barrionuevo G. 2001. Voltage-gated sodium channels shape subthreshold EPSPs in layer 5 pyramidal neurons from rat prefrontal cortex. J Neurophysiol. 86:1671–1684.

Han ZS, Buhl EH, Lorinczi Z, Somogyi P. 1993. A high degree of spatial selectivity in the axonal and dendritic domains of physiologically identified local-circuit neurons in the dentate gyrus of the rat hippocampus. Eur J Neurosci. 5:395–410.

Heinemann U, Beck H, Dreier JP, Ficker E, Stabel J, Zhang CL. 1992. The dentate gyrus as a regulated gate for the propagation of epileptiform activity. Epilepsy Res Suppl. 7:273–280.

Hong SE, Shugart YY, Huang DT, Shahwan SA, Grant PE, Hourihane JO, Martin ND, Walsh CA. 2000. Autosomal recessive lissencephaly with cerebellar hypoplasia is associated with human RELN mutations. Nat Genet. 26:93–96.

Ishida A, Shimazaki K, Terashima T, Kawai N. 1994. An electrophysiological and immunohistochemical study of the hippocampus of the *reeler* mutant mouse. Brain Res. 662:60–68.

Jack JJ. 1975. Physiology of peripheral nerve fibres in relation to their size. Br J Anaesth. 47(Suppl):173–182.

Kerr AM, Capogna M. 2007. Unitary IPSPs enhance hilar mossy cell gain in the rat hippocampus. J Physiol. 578:451–470.

Klausberger T, Somogyi P. 2008. Neuronal diversity and temporal dynamics: the unity of hippocampal circuit operations. Science. 321:53–57.

Larimer P, Strowbridge BW. 2008. Nonrandom local circuits in the dentate gyrus. J Neurosci. 28:12212–12223.
Liu WS, Pesold C, Rodriguez MA, Carboni G, Auta J, Lacor P, Larson J, Condie BG, Guidotti A, Costa E. 2001. Down-regulation of dendritic spine and glutamic acid decarboxylase 67 expressions in the reelin haploinsufficient heterozygous *reeler* mouse. Proc Natl Acad Sci USA. 98:3477–3482.
Liu Y, Fujise N, Kosaka T. 1996. Distribution of calretinin immunoreactivity in the mouse dentate gyrus. I. General description. Exp Brain Res. 108:389–403.
Lübke J, Frotscher M, Spruston N. 1998. Specialized electrophysiological properties of anatomically identified neurons in the hilar region of the rat fascia dentata. J Neurophysiol. 79:1518–1534.
Lysetskiy M, Földy C, Soltesz I. 2005. Long- and short-term plasticity at mossy fiber synapses on mossy cells in the rat dentate gyrus. Hippocampus. 15:691–696.
Niu S, Renfro A, Quattrocchi CC, Sheldon M, D'Arcangelo G. 2004. Reelin promotes hippocampal dendrite development through the VLDLR/ApoER2-Dab1 pathway. Neuron. 41:71–84.
Niu S, Yabut O, D'Arcangelo G. 2008. The Reelin signaling pathway promotes dendritic spine development in hippocampal neurons. J Neurosci. 28:10339–10348.
Pascual M, Perez-Sust P, Soriano E. 2004. The GABAergic septohippocampal pathway in control and *reeler* mice: target specificity and termination onto Reelin-expressing interneurons. Mol Cell Neurosci. 25:679–691.
Patrylo PR, Browning RA, Cranick S. 2006. *Reeler* homozygous mice exhibit enhanced susceptibility to epileptiform activity. Epilepsia. 47:257–266.
Patrylo PR, Willingham A. 2007. Anatomic and electrophysiologic evidence for a proconvulsive circuit in the dentate gyrus of *reeler* mutant mice, an animal model of diffuse cortical malformation. Dev Neurosci. 29:73–83.
Qui SF, Korwek KM, Pratt-Davis AR, Peters M, Bergman MY, Weeber EJ. 2006. Cognitive disruption and altered hippocampus synaptic function in Reelin haploinsufficient mice. Neurobiol Learn Mem. 85:228–242.
Ratzliff AH, Santhakumar V, Howard A, Soltesz I. 2002. Mossy cells in epilepsy: rigor mortis or vigor mortis? Trends Neurosci. 25:140–144.
Ribak CE, Seress L, Amaral DG. 1985. The development, ultrastructure and synaptic connections of the mossy cells of the dentate gyrus. J Neurocytol. 14:835–857.
Scharfman HE. 1991. Dentate hilar cells with dendrites in the molecular layer have lower thresholds for synaptic activation by perforant path than granule cells. J Neurosci. 11:1660–1673.
Scharfman HE. 1995. Electrophysiological diversity of pyramidal-shaped neurons at the granule cell layer/hilus border of the rat dentate gyrus recorded in vitro. Hippocampus. 5:287–305.
Scharfman HE, Schwartzkroin PA. 1988. Electrophysiology of morphologically identified mossy cells of the dentate hilus recorded in guinea pig hippocampal slices. J Neurosci. 8:3812–3821.
Schmidt-Hieber C, Jonas P, Bischofberger J. 2007. Subthreshold dendritic signal processing and coincidence detection in dentate gyrus granule cells. J Neurosci. 27:8430–8441.
Sloviter RS, Zappone CA, Harvey BD, Bumanglag AV, Bender RA, Frotscher M. 2003. Dormant basket cell" hypothesis revisited: relative vulnerabilities of dentate gyrus mossy cells and inhibitory interneurons after hippocampal status epilepticus in the rat. J Comp Neurol. 459:44–76.
Sotelo C. 1990. Cerebellar synaptogenesis: what we can learn from mutant mice. J Exp Biol. 153:225–249.
Spruston N, Jaffe DB, Johnston D. 1994. Dendritic attenuation of synaptic potentials and currents: the role of passive membrane properties. Trends Neurosci. 17:161–166.
Spruston N, Jaffe DB, Williams SH, Johnston D. 1993. Voltage- and space-clamp errors associated with the measurement of electrotonically remote synaptic events. J Neurophysiol. 70:781–802.
Stanfield BB, Cowan WM. 1979. The morphology of the hippocampus and dentate gyrus in normal and *reeler* mice. J Comp Neurol. 185:393–422.
Stirling RV, Bliss TV. 1978. Observations on the commissural projection to the dentate gyrus in the *Reeler* mutant mouse. Brain Res. 150:447–465.
Stuart G, Sakmann B. 1995. Amplification of EPSPs by axosomatic sodium channels in neocortical pyramidal neurons. Neuron. 15:1065–1076.
Vida I, Frotscher M. 2000. A hippocampal interneuron associated with the mossy fiber system. Proc Natl Acad Sci USA. 97:1275–1280.
Wen Q, Chklovskii DB. 2008. A cost-benefit analysis of neuronal morphology. J Neurophysiol. 99:2320–2328.
Williams SR, Mitchell SJ. 2008. Direct measurement of somatic voltage clamp errors in central neurons. Nat Neurosci. 11:790–798.
Zhao S, Förster E, Chai X, Frotscher M. 2003. Different signals control laminar specificity of commissural and entorhinal fibers to the dentate gyrus. J Neurosci. 23:7351–7357.